

RSC Advances



This is an *Accepted Manuscript*, which has been through the Royal Society of Chemistry peer review process and has been accepted for publication.

Accepted Manuscripts are published online shortly after acceptance, before technical editing, formatting and proof reading. Using this free service, authors can make their results available to the community, in citable form, before we publish the edited article. This *Accepted Manuscript* will be replaced by the edited, formatted and paginated article as soon as this is available.

You can find more information about *Accepted Manuscripts* in the [Information for Authors](#).

Please note that technical editing may introduce minor changes to the text and/or graphics, which may alter content. The journal's standard [Terms & Conditions](#) and the [Ethical guidelines](#) still apply. In no event shall the Royal Society of Chemistry be held responsible for any errors or omissions in this *Accepted Manuscript* or any consequences arising from the use of any information it contains.

Cite this: DOI: 10.1039/c0xx00000x

www.rsc.org/xxxxxx

ARTICLE TYPE

One-pot synthesis of hierarchical SnO₂ hollow nanospindles self-assembled from nanorods and their lithium storage properties

Qingjiang Yu,^{*ab} Wenqi Wang,^a Huixin Wang,^c Yuwu Huang,^a Jinzhong Wang,^{*a} Shiyong Gao,^{*a} Fengyun Guo,^a Xitian Zhang,^b Hong Gao,^b Xuanzhang Wang^b and Cuiling Yu^{*d}⁵ Received (in XXX, XXX) Xth XXXXXXXXX 20XX, Accepted Xth XXXXXXXXX 20XX

DOI: 10.1039/b000000x

Novel hierarchical SnO₂ hollow nanospindles self-assembled from nanorods have been successfully synthesized via a templating approach under hydrothermal conditions. The influence of the reactant concentration on SnO₂ products is investigated in detail. It is found that the interplay of the acidic etching of Fe₂O₃ templates and controlled hydrolysis of SnCl₂ is significant for the formation of the hierarchical SnO₂ hollow nanostructures. The evolution process and formation mechanism of the hollow structures with nanorods are analyzed from the angle of nucleation and morphology. Moreover, the electrochemical properties of the hollow structures are also studied by charge–discharge cycling, the result displays that the hierarchical SnO₂ hollow nanostructure exhibits much better lithium storage properties with higher reversible capacities and enhanced cyclic capacity retention than the commercial SnO₂ nanoparticles.

Introduction

SnO₂ is one of the most intensively investigated materials owing to its widespread applications in lithium-ion batteries,¹ gas sensors,² photocatalysts,³ and optoelectronic devices.⁴ So far, numerous efforts have been devoted to synthesizing various nanostructures of SnO₂, such as nanoparticles,⁵ nanorods,⁶ nanowires,⁷ nanobelts,⁸ nanotubes,⁹ nanosheets,¹⁰ hollow structures,^{11–15} and mesoporous structures.^{16–18}

In recent years, hollow structures have attracted considerable attention due to high surface area, low density, well-defined interior voids, and surface permeability.¹⁹ Controlled synthesis strategies for hollow structures have involved the use of templating or template-free methods. The template-free formation of hollow structures is usually based on the oriented attachment and inside-out Ostwald ripening.^{11,12,20} However, the morphological uniformity and interior complexity of hollow products are less controllable by this strategy. Although templating methods generally include multiple steps, they have been considered as the most representative and effective approach for the preparation of hollow structures with a narrow size distribution and well-defined shape.²¹ The controlled assembling of the designed materials on various removable templates, such as monodisperse silica/polymer latex spheres,^{22,23} emulsion micelles,²⁴ and even gas bubbles,²⁵ has been widely investigated. Nevertheless, the geometry of hollow structures obtained from template-engaged approaches is mostly spherical. While the preparation of non-spherical hollow structures still suffer from many difficulties in uniform coating around high-curvature surfaces and the paucity of non-spherical templates available.¹⁹ In this regard, several novel approaches in combination with sacrificial templates have been developed to synthesize various

hollow structures on the basis of different formation mechanisms, including the Kirkendall effect,²⁶ galvanic replacement,²⁷ chemical etching,²⁸ thermal decomposition,²⁹ etc. The sacrificial templates can directly determine the shape and cavity size of the resultant hollow structures by involving themselves as the consumable reactants for shell construction. Recently, Lou and co-workers have demonstrated the fast formation of SnO₂ nanoboxes with uniform morphology, good structural stability and tunable interior volume by template-engaged coordinating etching of pregrown Cu₂O nanocubes at room temperature.³⁰ Shortly after that, uniform polycrystalline SnO₂ hollow nanostructures with various shapes have also been synthesized by templating against shape-controlled α -Fe₂O₃ crystals under hydrothermal conditions.³¹

To date, the research for SnO₂ hollow structures mainly focuses on the control of the shape and hollow interior by engineering the templates, while tailoring of the outer shell structure remains a great challenge. Generally, the shells of SnO₂ hollow structures are comprised of zero-dimensional polycrystalline nanoparticles.^{11–15,30,31} However, constructing SnO₂ hollow nanostructures from building blocks of single-crystalline nanorods were rarely studied. Herein, we present one-step synthesis of hierarchical SnO₂ hollow nanospindles self-assembled from single-crystalline nanorods by utilizing α -Fe₂O₃ nanocrystals with non-spherical shapes as the sacrificial templates under hydrothermal conditions. The effects of the reactant concentration and reaction time on SnO₂ products are analyzed, and the formation mechanism of the hierarchical SnO₂ hollow nanostructure is discussed from the angle nucleation and morphology. Moreover, we also evaluate the electrochemical characteristics of the SnO₂ hollow nanospindles as lithium storage anodes for secondary lithium batteries.

Experimental

Material synthesis

The α -Fe₂O₃ nanospindles were synthesized by treating an aqueous solution of 20 mM FeCl₃·6H₂O and 0.35 mM NaH₂PO₄ at 105 °C for 48 h. In a typical synthesis process of SnO₂ hollow nanospindles, 0.02 g of α -Fe₂O₃ nanospindles was dispersed in 30 ml of an aqueous solution containing a 0.45 M HCl by ultrasonication for 10 min, followed by successively adding 0.05 g of SnCl₂·2H₂O powder under mild magnetic stirring for 10 min. Then the suspension was transferred into a 50 mL Teflon-lined stainless steel autoclave. The reaction was conducted at 180 °C for 20 h. Subsequently, the resulting products were centrifuged, and washed with deionized water and ethanol several times before being dried at 60 °C in air.

15 Characterization and electrochemical measurement

X-ray power diffraction (XRD) analysis was conducted on a Rigaku D/max-2500 X-ray diffractometer with Cu K α radiation ($\lambda=1.5418$ Å). Field emission scanning electron microscopic (FESEM) images were performed on a JEOL JEM-6700F microscope operating at 5 KV. Transmission electron microscope (TEM) and high-resolution TEM (HRTEM) observations were carried out with a JEOL JEM-2100 microscope operated at 200 KV. The Brunauer–Emmett–Teller (BET) surface area was determined by N₂ adsorption-desorption at 77 K using a BELSORP-max surface area analyzer. The electrochemical measurements were conducted by using two-electrode Swagelok-type cells with pure lithium foil as the counter and reference electrode at room temperature. The working electrode consisted of SnO₂ hollow nanospindles, conductivity agent (carbon black, Super-P-Li), and polyvinylidene difluoride (PVDF) in a weight ratio of 70:20:10. The electrolyte was 1.0 M LiPF₆ in a 50:50 (w/w) mixture of ethylene carbonate and diethyl carbonate. Cell assembly was carried out in an Ar-filled glovebox with concentrations of moisture and oxygen below 1.0 ppm. The galvanostatic charge–discharge tests were performed with a NEWARE battery tester at different current densities within a cutoff voltage window of 0.01–1.2 V. 1 C is equivalent to 782 mA g⁻¹, corresponding to 4.4 Li atoms per SnO₂ molecule.

Results and Discussion

The crystallographic structure of the as-prepared hollow nanospindles was determined by XRD, as shown in Fig. 1. All of the diffraction peaks can be perfectly indexed to tetragonal rutile SnO₂ (JCPDS card no. 41-1445, space group: *P4₂/mnm*, $a_0 = 4.7382$ Å, $c_0 = 3.1871$ Å).³² No diffraction peaks from other crystalline impurities were detected. The morphology of the obtained products was characterized by FESEM and TEM. Figure 2a shows a FESEM image displaying uniform nanospindles with an average length of around 415 nm. The hollow structure is clearly revealed from several broken nanospindles indicated by white arrows (Fig. 2a). The hollow structures of nanospindles are further confirmed by TEM, as shown in Fig. 2b. Interestingly, it is apparent that the entire hollow nanospindles are built from perpendicular one-dimension nanorods with ~34 nm in length and ~7 nm in diameter (Fig. 2c). It is noteworthy to stress that these hollow nanospindles are sufficiently stable and could not be

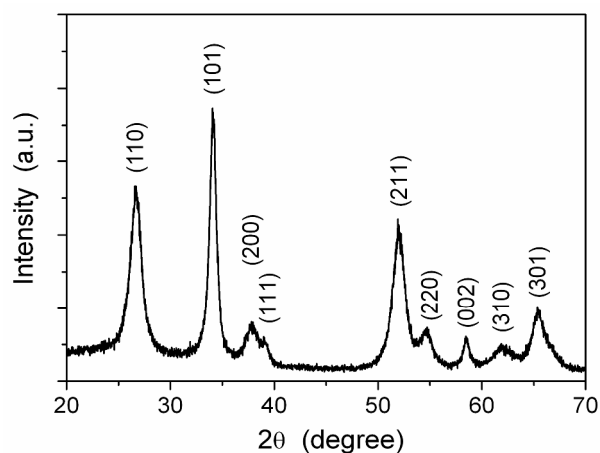


Fig. 1 XRD pattern of the SnO₂ hollow nanospindles.

destroyed even after longtime ultrasonication. To further study the fine structure of the nanorods, a representative HRTEM image of a single nanorod is given in Fig. 2d. The clear lattice fringes in the HRTEM image indicate that the nanorod is a single crystal. The interplanar spacings are about 0.335 and 0.264 nm, corresponding to (110) and (101) planes of rutile SnO₂, respectively, suggesting that the growth direction of the nanorods is along [1–12].³³

To investigate the effect of the reactant concentration, we first changed the concentration of HCl while keeping the content of SnCl₂ (0.05 g). Fig. 3 displays the morphologies of the synthesized products at different reaction concentrations. When the concentration of HCl is 0.15 M, the Fe₂O₃ templates are not dissolved due to a lower concentration of HCl. Large quantities of SnO₂ nanoparticles (3~6 nm in diameter) are formed on the surface or outside of Fe₂O₃ nanospindles, as shown in Fig. 3a. When the HCl concentration is increased to 0.25 M, the continuous shells consisting of SnO₂ nanoparticles (2~3 nm in diameter) are formed around the scaffold of Fe₂O₃ nanospindles while the Fe₂O₃ cores are partially dissolved (Fig. 3b). As the HCl concentration is added to 0.35 M, the Fe₂O₃ templates are almost eliminated and the SnO₂ hollow nanospindles are obtained. It can

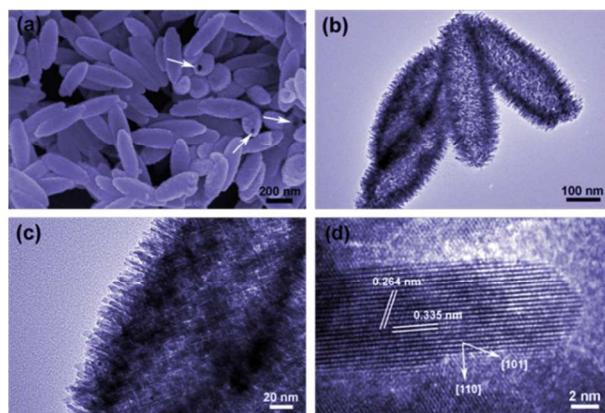


Fig. 2 (a and b) FESEM and TEM images of SnO₂ hollow nanospindles. (c) high-magnification TEM image recorded around the edge of a SnO₂ hollow nanospindle with vertical nanorods. (d) high-resolution TEM image of a single nanorod.

be obviously observed that the shells of these hollow nanospindles are comprised of nanorod arrays with ~ 13 nm in length (Fig. 3c). By further increasing the HCl concentration, these vertical nanorods gradually grow up (Fig. 2). Once the HCl concentration is increased to 0.55 M, imperfect hollow nanospindles are obtained, as displayed in Fig. 3d. This may be attributed to the fast dissolution of the Fe_2O_3 templates due to a higher HCl concentration, leading to forming large amounts of unordered nanorods. Moreover, we also changed the content of SnCl_2 while keeping the HCl concentration (0.45 M). At a low content of SnCl_2 (0.02 g), the SnO_2 hollow nanospindles are built from smaller nanorods with lengths of ~ 22 nm, as shown in Fig. 3e. When the content of SnCl_2 is added to 0.08 g, the building blocks of hollow nanospindles are not one-dimensional nanorods but some irregular nanoparticles (Fig. 3f). This possible reason will be described below.

To understand the formation process of the SnO_2 hollow nanospindles comprised of vertical nanorods, the products were synthesized at different reaction times. Fig. 4 shows the evolution of the SnO_2 hollow nanospindles as a function of reaction time. TEM observation of the product, which aged 180°C for 0.5 h, reveals that SnO_2 nanoparticles with ~ 2 nm in diameter are formed on the surface of Fe_2O_3 templates which are not almost changed (Fig. 4a). As the reaction time is prolonged to 3 h, the Fe_2O_3 templates are partially dissolved by HCl etching and the shells formed around the scaffold of Fe_2O_3 templates are comprised of SnO_2 nanoparticles and small nanorods (~ 8 nm in length and ~ 3 nm in diameter), as displayed in Fig. 4b. Upon prolonging the reaction time, the size of the nanorods obviously increase while the nanoparticles disappear (Fig. 4c), which indicates that the nanoparticles are only an intermediate and will gradually form nanorods with increasing the reaction time. After

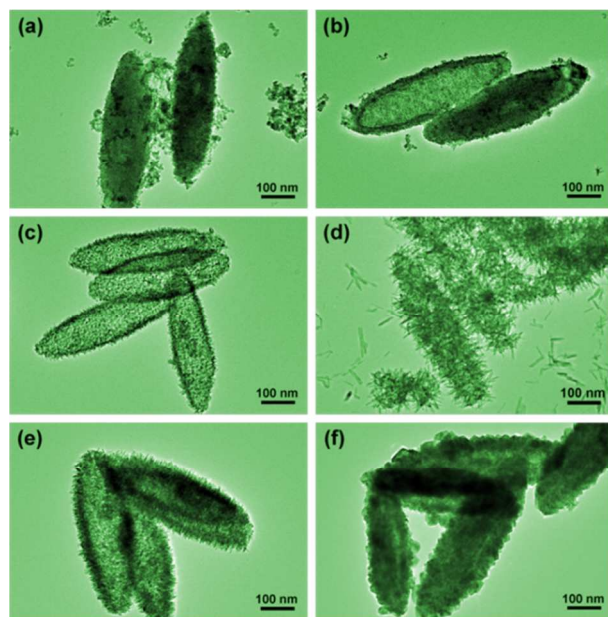


Fig. 3 (a-d) TEM images of the products obtained with different HCl concentrations: (a) 0.15 M, (b) 0.25 M, (c) 0.35 M, and (d) 0.55 M. (e and f) TEM images of the products obtained with various SnCl_2 contents: (e) 0.02 g, and (f) 0.08 g.

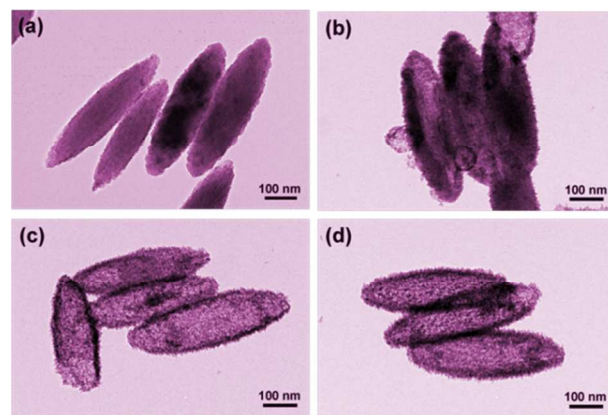
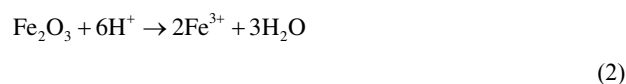
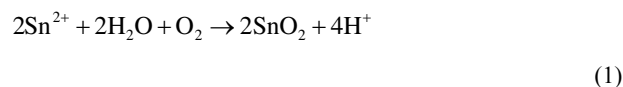


Fig. 4 TEM images of the products prepared at different reaction times: (a) 0.5 h, (b) 3 h, (c) 8 h, and (d) 12 h.

reaction for 12 h, the Fe_2O_3 templates are almost removed (Fig. 4d) and the SnO_2 hollow nanospindles with perpendicular nanorods are achieved after 20 h (Fig. 2). The effect of longer reaction times, up to 30 h, was also investigated. Results show that the reaction time exceeding 20 h will not bring about evident morphological modifications.

On the basis of the experimental results mentioned above, the following chemical reactions may take place during the formation of the SnO_2 hollow nanospindles with nanorods.³¹



In this reaction, Sn^{2+} reacts with oxygen in the solution under the hydrothermal conditions to yield insoluble SnO_2 (Eq. 1). At the early stage of the reaction, SnO_2 will nucleate on the surface of Fe_2O_3 templates due to the mutual crystallographic compatibility. Subsequently, the SnO_2 nuclei grow duratively and further evolve a precipitation layer. Meanwhile, the Fe_2O_3 templates are gradually dissolved in the acidic solution (Eq. 2). The SnO_2 hollow nanostructures are ultimately formed after entire etching of the Fe_2O_3 templates. In the reaction solution, HCl plays a key role in the formation of the SnO_2 hollow nanospindles covered by nanorods, because it can kinetically control the hydrolysis of Sn^{2+} and the dissolution of Fe_2O_3 templates. Moreover, at a given content of Sn^{2+} , a higher concentration of HCl is beneficial to the

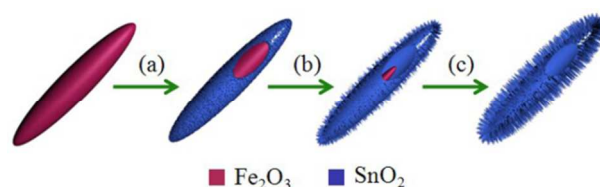


Fig. 5 Schematic sketch of the formation process of SnO_2 hollow nanospindles with nanorods: (a) heterogeneous nucleation of SnO_2 grains around the scaffold of Fe_2O_3 crystals; (b) growth of SnO_2 nanorods and simultaneous dissolution of Fe_2O_3 cores by HCl etching; and (c)

formation of SnO₂ hollow nanospindles with nanorods after complete consumption of Fe₂O₃ crystals.

formation of SnO₂ nanorods, which is because Cl⁻ may absorb preferentially on (110) crystal faces of SnO₂ and prevent the growth rate of these surfaces.³⁴ However, at a higher Sn²⁺ concentration, the more SnO₂ nuclei appear simultaneously at beginning of the reaction and congregate easily under hydrothermal conditions, which will attenuate the influence of Cl⁻ on retarding the growth rate of SnO₂ (110) crystal faces, leading to the formation of irregular SnO₂ nanoparticles. The formation process of SnO₂ hollow nanospindles with nanorods can be schematically summarized in Fig. 5.

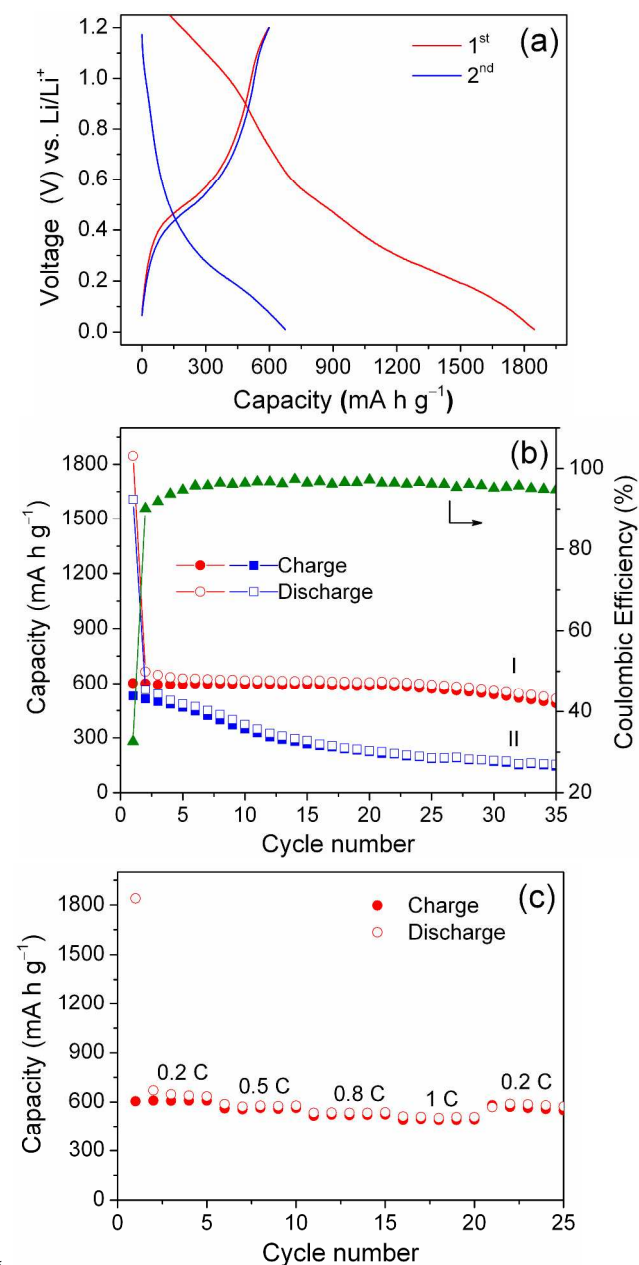
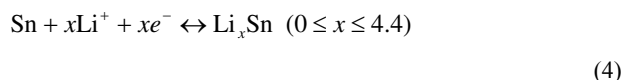
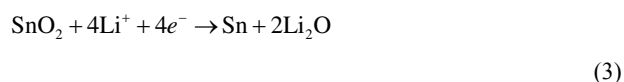


Fig. 6 (a) Charge-discharge profiles of SnO₂ hollow nanospindles at a current rate of 0.2 C for the first and second cycles. (b) Cycling performance of SnO₂ hollow nanospindles (I) and commercial SnO₂ nanoparticles (II) and coulombic efficiency of SnO₂ hollow nanospindles

at a current rate of 0.2 C. (c) Cycling performance of SnO₂ hollow nanospindles at various current rates.

SnO₂ has been intensively investigated as a promising anode material for the next generation lithium-ion batteries.^{10,35–38} The lithium storage mechanism of SnO₂ can be described by the following two reactions:^{35,36}



The lithium storage capability of SnO₂ is dependent on the reversible alloying-dealloying processes between lithium and metallic Sn nanocrystals (Eq. 4) which are generated from the initial irreversible reduction of SnO₂ (Eq. 3). Although SnO₂ has an attractive theoretical capacity of ~781 mA h g⁻¹,⁴⁰ a major hindrance against the commercial use of SnO₂-based anode materials in lithium-ion batteries is large volume and uneven changes during the lithium alloying and dealloying processes, which leads to poor cycling capability.^{36,40,41} Recently, increasing evidence has indicated that use of hollow structures could effectively alleviate the so-called pulverization problem and enhance the kinetics and structural stability for lithium storage.^{12,14,30,31} Motivated by this interest, we have carried out preliminary electrochemical characterization using the SnO₂ hollow nanospindles as anode materials for lithium-ion batteries.

Fig. 6a displays representative discharge-charge voltage profiles of SnO₂ hollow nanospindles in the range of 0.01–1.2 V at 0.2 C. The voltage window of 0.01–1.2 V was chosen in order to partly prevent the surface reaction between Sn and Li₂O which occurs at higher voltage and minimize solid electrolyte interface (SEI) formation on Sn.^{41,42} The initial discharge and charge capacities are 1850 and 602 mA h g⁻¹, respectively. Such a large capacity loss in the first cycle is often ascribed to the irreversible reduction of some lithium in the lattice and inevitable formation of SEI layer.^{30,31,40–42} Fig. 6b depicts the cycling performance of SnO₂ hollow nanospindles and commercial SnO₂ nanoparticles up to 35 cycles. In view of the initial irreversible loss, there is a large drop in capacity of the 2th cycle for both samples. It is found that SnO₂ hollow nanospindles exhibit a high discharge capacity of 516 mA h g⁻¹ after 35 cycles, which is much higher than the theoretical capacity of graphite (372 mA h g⁻¹). From the fourth cycle onward, the SnO₂ hollow nanospindles display a high Coulombic efficiency of about 95%. However, the discharge capacity decays rapidly to less than 300 mA h g⁻¹ after 15 cycles for the commercial SnO₂ nanoparticles. It is suggested that such SnO₂ hierarchical structure could prevent dense aggregation of the nanorod building blocks and provide a more stable porous structure. The pores and void space between nanorods could effectively accommodate the large volume expansion or contraction during the discharge-charge processes, which would probably better retain the integrity of the electrode. Furthermore, the hierarchical structure with a larger surface area of 79 m² g⁻¹ (Fig. S1) could increase a big contact area with the electrolyte and enhance the Li⁺ ion transfer rate during cycling. To investigate the rate capability, our SnO₂ hollow nanospindle

electrode was discharged and charged at various current rates, as shown in Fig. 6c. The specific capacity slightly decreases with an increase in the current rate, and it still displays a discharge capacity of above 490 mA h g⁻¹ at 1 C. When the current rate is returned to 0.2 C, the capacity of about 585 mA h g⁻¹ can be resumed.

Conclusions

In summary, we have been successfully synthesized uniform hierarchical SnO₂ hollow nanospindles self-assembled from nanorods by templating against α -Fe₂O₃ nanocrystals under hydrothermal conditions. The fine-tuned interact between the acidic etching of Fe₂O₃ templates and hydrolysis of SnCl₂ is crucial for the formation of this novel SnO₂ hollow nanostructure. The evolution process and formation mechanism of the SnO₂ hollow nanospindles are discussed from the angle of nucleation and morphology. When evaluated for their lithium storage properties, the SnO₂ hollow nanospindles manifest higher specific discharge capacity and better cycling ability compared to the commercial SnO₂ nanoparticles. The enhanced electrochemical properties may be due to the unique nanostructure which provide good structural stability and improve Li⁺ ion transfer rate. It is believed that such hierarchical SnO₂ hollow structures are also promising in other applications such as photocatalysis, gas sensors, and dye-sensitized solar cells.

Acknowledgments

We gratefully acknowledge financial support from the National 863 Project (No. 2013AA031502) the National Natural Science Foundation of China (No. 51202046), the Fundamental Research Funds for the Central Universities (Nos. HIT.NSRIF.2013006 and HIT.BRETHIII.201403), the China Postdoctoral Science Foundation (Nos. 2012M510144 and 2013T60366), and the Open Project Program of Key Laboratory for Photonic and Electric Bandgap Materials, Ministry of Education, Harbin Normal University, China. We are also grateful to Prof. Chengyan Xu for useful discussions.

Notes and references

^aDepartment of Optoelectric Information Science, School of Materials Science and Engineering, Harbin Institute of Technology, Harbin, 150001, China. Fax: +86 451 86418328; Tel: +86 451 86417763; E-mail: qingjiang.yu@hit.edu.cn; jinzhong_wang@hit.edu.cn; gaoshiyong@hit.edu.cn

^bKey Laboratory for Photonic and Electric Bandgap Materials, Ministry of Education, Harbin Normal University, Harbin, 150025, China

^cDepartment of Material Physics and Chemistry, School of Materials Science and Engineering, Harbin Institute of Technology, Harbin, 150001, China

^dDepartment of Physics, Harbin Institute of Technology, Harbin, 150001, China. E-mail: cuiling.yu@hit.edu.cn

† Electronic Supplementary Information (ESI) available: N₂ adsorption-desorption isotherms of SnO₂ hollow nanospindles. See DOI: 10.1039/b000000x/

1 S. Han, B. Jang, T. Kim, S. M. Oh and T. Hyeon, *Adv. Funct. Mater.*, 2005, **15**, 1845.

2 A. Kolmakov, Y. Zhang, G. Cheng and M. Moskovits, *Adv. Mater.*, 2003, **15**, 997.

3 Z. Liu, D. D. Sun, P. Guo and J. O. Leckie, *Nano Lett.*, 2007, **7**, 1081.

4 H. J. Snaith and C. Ducati, *Nano Lett.*, 2010, **10**, 1259.

- 5 V. Juttukonda, R. L. Paddock, J. E. Raymond, D. Denomme, A. E. Richardson, L. E. Slusher and B. D. Fahlman, *J. Am. Chem. Soc.*, 2006, **128**, 420.
- 6 D. F. Zhang, L. D. Sun, J. L. Yin, C. H. Yan, *Adv. Mater.*, 2003, **15**, 1022.
- 7 M. S. Park, G. X. Wang, Y. M. Kang, D. Wexler, S. X. Dou and H. K. Liu, *Angew. Chem. Int. Ed.*, 2007, **46**, 750.
- 8 Z. W. Pan, Z. R. Dai and Z. L. Wang, *Science*, 2001, **291**, 1947.
- 9 P. Wu, N. Du, H. Zhang, J. Xu, Y. Qi and D. Yang, *Nanoscale*, 2011, **3**, 746.
- 10 C. Wang, Y. Zhou, M. Y. Ge, X. B. Xu, Z. L. Zhang and J. Z. Jiang, *J. Am. Chem. Soc.*, 2010, **132**, 46.
- 11 H. G. Yang and H. C. Zeng, *Angew. Chem. Int. Ed.*, 2004, **43**, 5930.
- 12 X. W. Lou, Y. Wang, C. L. Yuan, J. Y. Lee and L. A. Archer, *Adv. Mater.*, 2006, **18**, 2325.
- 13 J. G. Yu, H. T. Guo, S. A. Davis and S. Mann, *Adv. Funct. Mater.*, 2006, **16**, 2035.
- 14 J. S. Chen, C. M. Li, W. W. Zhou, Q. Y. Yan, L. A. Archer and X. W. Lou, *Nanoscale*, 2009, **1**, 280.
- 15 W. Wu, S. Zhang, J. Zhou, X. Xiao, F. Ren and C. Jiang, *Chem. Eur. J.*, 2011, **17**, 9708.
- 16 J. H. Ba, J. Polleux, M. Antonietti and M. Niederberger, *Adv. Mater.*, 2005, **17**, 2509.
- 17 N. Tatsuda, T. Nakamura, D. Yamamoto, T. Yamazaki, T. Shimada, H. Inoue and K. Yano, *Chem. Mater.*, 2009, **21**, 5252.
- 18 Z. Li, Q. Zhao, W. Fan and J. Zhan, *Nanoscale*, 2011, **3**, 1646.
- 19 X. W. Lou, L. A. Archer and Z. Yang, *Adv. Mater.*, 2008, **20**, 3987.
- 20 R. L. Penn and J. F. Banfield, *Science*, 1998, **281**, 969.
- 21 P. Jiang, J. F. Bertone and V. L. Colvin, *Science*, 2001, **291**, 453.
- 22 Z. Zhong, Y. Yin, B. Gates and Y. Xia, *Adv. Mater.*, 2000, **12**, 206.
- 23 F. Caruso, R. A. Caruso and H. Mohwald, *Science*, 1998, **282**, 1111.
- 24 C. I. Zoldesi and A. Imhof, *Adv. Mater.*, 2005, **17**, 924.
- 25 Q. Peng, Y. Dong and Y. Li, *Angew. Chem. Int. Ed.*, 2003, **42**, 3027.
- 26 Y. D. Yin, R. M. Rioux, C. K. Erdonmez, S. Hughes, G. A. Somorjai and A. P. Alivisatos, *Science*, 2004, **304**, 711.
- 27 Y. G. Sun and Y. N. Xia, *Science*, 2002, **298**, 2176.
- 28 M. Hu, A. A. Belik, M. Imura and Y. Yamauchi, *J. Am. Chem. Soc.*, 2013, **135**, 384.
- 29 W. Cho, Y. H. Lee, H. J. Lee and M. Oh, *Adv. Mater.*, 2011, **23**, 1720.
- 30 Z. Wang, D. Luan, F. Y. C. Boey and X. W. Lou, *J. Am. Chem. Soc.*, 2011, **133**, 4738.
- 31 Z. Wang, Z. C. Wang, S. Madhavi and X. W. Lou, *Chem. Eur. J.*, 2012, **18**, 7561.
- 32 B. Cheng, J. M. Russell, W. Shi, L. Zhang and E. T. Samulski, *J. Am. Chem. Soc.*, 2004, **126**, 5972.
- 33 P. Sun, L. You, Y. Sun, N. Chen, X. Li, H. Sun, J. Ma and G. Lu, *CrystEngComm*, 2012, **14**, 1701.
- 34 Y.-L. Wang, M. Guo, M. Zhang and X.-D. Wang, *CrystEngComm*, 2010, **12**, 4024.
- 35 X. W. Lou, C. M. Li and L. A. Archer, *Adv. Mater.*, 2009, **21**, 2536.
- 36 M. G. Km and J. Cho, *Adv. Funct. Mater.*, 2009, **19**, 1497.
- 37 P. Wu, N. Du, H. Zhang, C. Zhai and D. Yang, *ACS Appl. Mater. Interfaces*, 2011, **3**, 1946.
- 38 M. Zhang, Y. Li, E. Uchaker, S. Candelaria, L. Shen, T. Wang and G. Cao, *Nano Energy*, 2013, **2**, 769.
- 39 J. Li, P. Wu, Y. Ye, H. Wang, Y. Zhou, Y. Tang and T. Lu, *CrystEngComm*, 2014, **16**, 517.
- 40 I. A. Courtney and J. R. Dahn, *J. Electrochem. Soc.*, 1997, **144**, 2045.
- 41 I. A. Courtney, J. R. Dahn, *J. Electrochem. Soc.*, 1997, **144**, 2943.
- 42 I. T. Lucas, E. Pollak, R. Kostecki, *Electrochem. Commun.*, 2009, **11**, 2157.